

# Fluctuations in 21cm Emission After Reionization

J. Stuart B. Wyithe<sup>1</sup> and Abraham Loeb<sup>2</sup>

<sup>1</sup> *School of Physics, University of Melbourne, Parkville, Victoria, Australia*

<sup>2</sup> *Harvard-Smithsonian Center for Astrophysics, 60 Garden St., Cambridge, MA 02138*

*Email: swyithe@physics.unimelb.edu.au, loeb@cfa.harvard.edu*

28 October 2018

## ABSTRACT

The fluctuations in the emission of redshifted 21cm photons from neutral intergalactic hydrogen will provide an unprecedented probe of the reionization era. Conventional wisdom assumes that this 21cm signal disappears as soon as reionization is complete, when little atomic hydrogen is left through most of the volume of the intergalactic medium (IGM). However observations of damped Ly $\alpha$  absorbers indicate that the fraction of hydrogen in its neutral form is significant by mass at all redshifts. Here we use a physically-motivated model to show that residual neutral gas, confined to dense regions in the IGM with a high recombination rate, will generate a significant post-reionization 21cm signal. We show that the power-spectrum of fluctuations in this signal will be detectable by the first generation of low-frequency observatories at a signal-to-noise that is comparable to that achievable in observations of the reionization era. The statistics of 21cm fluctuations will therefore probe not only the pre-reionization IGM, but rather the entire process of HII region overlap, as well as the appearance of the diffuse ionized IGM.

**Key words:** cosmology: diffuse radiation, large scale structure, theory – galaxies: high redshift, intergalactic medium

## 1 INTRODUCTION

The reionization of cosmic hydrogen by the first stars and quasars (e.g. Barkana & Loeb 2001), was an important milestone in the history of the Universe. The recent discovery of distant quasars has allowed detailed absorption studies of the state of the high redshift intergalactic medium (IGM) at a time when the universe was less than a billion years old (Fan et al. 2006; White et al. 2003). Several studies have used the evolution of the ionizing background inferred from these spectra to argue that the reionization of cosmic hydrogen was completed just beyond  $z \sim 6$  (Fan et al. 2006; Gnedin & Fan 2006; White et al. 2003). However, other authors have claimed that the evidence for this rapid change becomes significantly weaker for a different choice of density distribution in the IGM (Becker et al. 2007). Different arguments in favour of a rapidly evolving IGM at  $z > 6$  are based on the properties of the putative HII regions inferred around the highest redshift quasars (Wyithe & Loeb 2004; Wyithe, Loeb, & Carilli 2005; Mesinger & Haiman 2005). However, Bolton & Haehnelt (2007a) and Lidz et al. (2007) have demonstrated that the interpretation of the spectral features is uncertain and that the observed spectra could either be produced by an HII region, or by a classical proximity zone. One reason for the ambiguity in interpreting

these absorption spectra is that Ly $\alpha$  absorption can only be used to probe neutral fractions that are smaller than  $10^{-3}$  owing to the large cross-section of the Ly $\alpha$  resonance.

A better probe of the process of reionization is provided by redshifted 21cm observations. Reionization starts with ionized (HII) regions around galaxies, which later grow to surround groups of galaxies. The process of reionization is completed when these HII regions overlap (defining the so-called *overlap* epoch) and fill-up most of the volume between galaxies. The conventional wisdom is that the 21cm signal disappears after the *overlap* epoch, because there is little neutral hydrogen left through most of intergalactic space. However, the following simple estimate can be used to demonstrate that 21cm emission should be significant even after reionization is completed. Damped Ly $\alpha$  systems are believed to contain the majority of the neutral gas at high redshifts. Indeed, observations of damped Ly $\alpha$  systems out to a redshift of  $z \sim 4$  show the cosmological density parameter of HI to be  $\Omega_{\text{HI}} \sim 10^{-3}$  (Prochaska et al 2005). In the standard cosmological model the density parameter of baryons is  $\Omega_{\text{b}} \sim 0.04$ , so that the mass-averaged neutral hydrogen fraction at  $z \sim 4$  (long after the end of the HII overlap epoch) is  $f_{\text{m}} \sim 0.03$ . This neutral gas does not contribute significantly to the effective Ly $\alpha$  optical depth, which is sensitive to the volume averaged neutral fraction

(with a value that is orders of magnitude lower). However the redshifted 21cm emission is sensitive to the total (mass-weighted) optical depth of this neutral gas. Observations of the redshifted 21cm signal would therefore detect the total neutral hydrogen content in a volume of IGM dictated by the observatory beam and frequency band-pass.

Although the 21cm emission after HII overlap is dominated by dense clumps of gas rather than by diffuse gas in the IGM as is the case before reionization is complete, we do not expect 21cm self absorption to impact the level of 21cm emission. This conclusion is based on 21cm absorption studies towards damped Ly $\alpha$  systems at a range of redshifts between  $z \sim 0$  and  $z \sim 3.4$ , which show optical depths to absorption of the back-ground quasar flux with values less than a few percent (Kanekar & Chengalur 2003; Curran et al. 2007). The small optical depth for self absorption is also supported by theoretical calculations of the 21cm optical depth of neutral gas in high redshift mini-halos (Furlanetto & Loeb 2002). Moreover, damped Ly $\alpha$  systems have a spin temperature that is large relative to the temperature of the cosmic microwave background radiation, and will therefore have a level of emission that is independent of the kinetic gas temperature (e.g. Kanekar & Chengalur 2003).

At  $z \sim 4$ , the brightness temperature contrast of redshifted 21cm emission will be  $\Delta T \sim 0.5\text{mK}$ . Moreover on the  $R \sim 10$  co-moving Mpc (hereafter cMpc) scales relevant for upcoming 21cm experiments, the *root-mean-square* amplitude of density fluctuations at  $z \sim 4$  is  $\sigma \sim 0.2$ . Hence, we expect fluctuations in the radiation field of  $\sim 0.1\text{mK}$  on 10 cMpc scales. The fluctuations in the 21cm emission signal after reionization are therefore expected to be only an order of magnitude or so smaller than the largest fluctuations predicted at any time during the entire reionization era (e.g. Wyithe & Morales 2007). In addition the sky temperature, which provides the limiting factor in the system noise at the low frequencies relevant for 21cm studies, is proportional to  $(1+z)^{2.6}$ , and so is a factor of  $\sim 3.4[(1+z)/5]^{2.6}$  smaller at low-redshifts than for observations at  $z \sim 7$ . Thus, detectability of fluctuations in 21cm emission may not decline substantially following the overlap epoch, allowing the study of the entire HII overlap process in redshifted 21cm emission.

In this paper we calculate the mean level of 21cm emission through the overlap epoch to lower redshifts, as well as the statistics of the fluctuations about this mean due to patchy reionization and fluctuations in the density field. Throughout the paper we adopt the set of cosmological parameters determined by *WMAP3* (Spergel et al. 2007) for a flat  $\Lambda$ CDM universe.

## 2 SEMI-ANALYTIC MODEL FOR REIONIZATION

Miralda-Escude et al. (2000) presented a model which allows the calculation of an effective recombination rate in an inhomogeneous universe by assuming a maximum overdensity ( $\Delta_c$ ) penetrated by ionizing photons within HII regions. The model assumes that reionization progresses rapidly through islands of lower density prior to the overlap of individual cosmological ionized regions. Following the overlap epoch, the remaining regions of high density are gradually ionized. It is therefore hypothesized that at any time, regions with gas be-

low some critical overdensity  $\Delta_i \equiv \rho_i/\langle\rho\rangle$  are highly ionized while regions of higher density are not. In what follows, we draw primarily from their prescription and refer the reader to the original paper for a detailed discussion of its motivations and assumptions. Wyithe & Loeb (2003) employed this prescription within a semi-analytic model of reionization. This model was extended by Srbinovsky & Wyithe (2006) and by Wyithe, Bolton & Haehnelt (2007). We refer the reader to those papers and only summarise the basics of the model below. In the current work we limit our attention to reionization due to population-II stars (Gnedin & Fan 2006; Srbinovsky & Wyithe 2006), which govern the final stages of reionization even in the presence of an earlier partial or full reionization by population III stars (e.g. Wyithe & Loeb 2003).

Within the model of Miralda-Escude et al. (2000) we describe the post-overlap evolution of the IGM by computing the evolution of the fraction of mass in regions with overdensity below  $\Delta_i$ ,

$$F_M(\Delta_i) = \int_0^{\Delta_i} d\Delta P_V(\Delta)\Delta, \quad (1)$$

where  $P_V(\Delta)$  is the volume weighted probability distribution for  $\Delta$ . In a region of large scale overdensity  $\delta$  at  $z_{\text{obs}}$ , the mass fraction  $F_M(\Delta_i)$  [or equivalently  $\Delta_i$ ] therefore evolves according to the equation

$$\frac{dF_M(\Delta_i)}{dz} = \frac{1}{n_0} \frac{dn_\gamma(\delta)}{dz} - \alpha_B \frac{R(\Delta_i)}{a^3} n_e \left( 1 + \delta \frac{D(z)}{D(z_{\text{obs}})} \right) \frac{dt}{dz}, \quad (2)$$

where  $D$  is the growth factor of linear density fluctuations,  $\alpha_B$  is the case B recombination coefficient,  $n_e$  is the comoving electron density,  $R(\Delta_i)$  is the effective clumping factor of the IGM (see below), and  $dn_\gamma/dz$  is the co-moving emissivity of ionizing photons. This equation was described in Wyithe & Loeb (2003), but is generalized here and below to regions of large scale overdensity  $\delta$  that differ from the average IGM (Wyithe, Bolton & Haehnelt 2007). Integration of equation (2) requires knowledge of  $P_V(\Delta)$ . Miralda-Escude et al. (2000) quote a fitting function which provides a good fit to the volume weighted probability distribution for the baryon density in cosmological hydrodynamical simulations. This probability distribution remains a reasonable description at high redshift when confronted with a more modern cosmology and updated simulations, although the addition of an analytical approximation for the high density tail of the distribution remains necessary as a best guess at correcting for numerical resolution (Bolton & Haehnelt 2007b).

Equation (2) provides a good description of the evolution of the ionization fraction following the overlap epoch of individual ionized bubbles, because the ionization fronts are exposed to the mean ionizing radiation field. However prior to the overlap epoch, the prescription is inadequate, due to the large fluctuations in the intensity of the ionizing radiation. A more accurate model to describe the evolution of the ionized volume prior to the overlap epoch was suggested by Miralda-Escude et al. (2000). In our notation the

appropriate equation is

$$\begin{aligned} \frac{dQ_i}{dz} &= \frac{1}{n^0 F_M(\Delta_{\text{crit}})} \frac{dn_\gamma(\delta)}{dz} \\ &- \left[ \alpha_B (1+z)^3 R(\Delta_{\text{crit}}) n_e \left( 1 + \delta \frac{D(z)}{D(z_{\text{obs}})} \right) \frac{dt}{dz} \right. \\ &\quad \left. + \frac{dF_M(\Delta_{\text{crit}})}{dz} \right] \frac{Q_i}{F_M(\Delta_c)}. \end{aligned} \quad (3)$$

In this expression,  $Q_i$  is redefined to be the volume filling factor within which all matter at densities below  $\Delta_c$  has been ionized, and  $R$  is the effective clumping of the IGM

Within this formalism, the epoch of overlap is precisely defined as the time when  $Q_i$  reaches unity. However, we have only a single equation to describe the evolution of two independent quantities  $Q_i$  and  $F_M$  (or equivalently  $\Delta_c$ ). The relative growth of these depends on the luminosity function and spatial distribution of the sources. The appropriate value of  $\Delta_c$  is set by the mean separation of the ionizing sources. We assume  $\Delta_c$  to be constant with redshift before the overlap epoch and compute results for models with values of  $\Delta_c = 20$  and  $\Delta_c = 5$ . Prior to reionization, these values imply a mean-free path that is comparable to the separation between galaxies (Wyithe & Loeb 2003). Our approach is to compute a reionization history given a particular value of  $\Delta_c$ , combined with assumed values for the efficiency of star-formation and the fraction of ionizing photons that escape from galaxies. With this history in place we then compute the evolution of the background radiation field due to these same sources. After the overlap epoch, ionizing photons will experience attenuation due to residual overdense pockets of HI gas. We use the description of Miralda-Escude et al. (2000) to estimate the ionizing photon mean-free-path, and subsequently derive the attenuation of ionizing photons. We then compute the flux at the Lyman-limit in the IGM due to sources immediate to each epoch, in addition to redshifted contributions from earlier epochs.

We next describe our model for the emissivity of population-II stars. Following Wyithe & Loeb (2003) we assume the spectral energy distribution (SED) of population-II star forming galaxies, using the model presented in Leitherer et al. (1999). From this SED we calculate the number of ionizing photons produced per baryon ( $N_\gamma$ ). Note that we ignore helium reionization in our modeling. We further assume that ionizing photons are produced primarily in starbursts, with lifetimes much shorter than the Hubble time, so that we may express the star formation rate per unit volume as

$$\frac{d\dot{M}}{dV}(z) = f_\star \frac{dF(\delta, z)}{dt_{\text{year}}} \rho_b, \quad (4)$$

where  $\rho_b$  is the co-moving baryonic mass density, and  $F(\delta, z)$  is the density dependent collapsed fraction of mass in halos above a critical mass at  $z$ . The factor  $f_\star$  (star formation efficiency) describes the fraction of collapsed baryonic matter that participates in star formation.

In a region of co-moving radius  $R$  and mean overdensity  $\delta(z) = \delta[D(z)/D(z_{\text{obs}})]$  [specified at redshift  $z$  instead of the usual  $z = 0$ ], the relevant collapsed fraction is obtained from the extended Press-Schechter (1974) model (Bond et

al. 1991) as

$$F(\delta, R, z) = \text{erfc} \left( \frac{\delta_c - \delta(z)}{\sqrt{2([\sigma_{\text{gal}}]^2 - [\sigma(R)]^2)}} \right), \quad (5)$$

where  $\text{erfc}(x)$  is the error function,  $\sigma(R)$  is the variance of the density field smoothed on a scale  $R$ , and  $\sigma_{\text{gal}}$  is the variance of the density field smoothed on a scale  $R_{\text{gal}}$ . The latter scale corresponds to the minimum halo mass for star-formation, and both variances are evaluated at redshift  $z$  rather than at  $z = 0$ . In this expression, the critical linear overdensity for the collapse of a spherical top-hat density perturbation is  $\delta_c \approx 1.69$ .

Prior to the redshift of the overlap epoch, the relevant scale  $R$  in the calculation of the biased collapsed fraction (equation 5) is equal to the size of the region being considered. However, following the overlap epoch the ionizing photon mean-free-path increases rapidly and quickly exceeds this scale. Once the mean-free-path is large, the ionizing photons contributing to the background within a region of size  $R$  were not produced locally. At times when the mean-free-path  $\lambda$  is greater than  $R$  we therefore assume that a fraction  $1 - R^3/\lambda^3$  of the ionizing background within a region of radius  $R$  was produced from sources in the mean-universe (we expect the contribution of the ionizing background from outside  $R$  to be only weakly correlated with the density of the region within  $R$  when  $\lambda \gg R$ ). The remaining fraction ( $R^3/\lambda^3$ ) is computed assuming biased star formation using equation (5). Note that this dilution applies only to the ionizing background, and not to the density of baryons within the region of size  $R$ .

In a cold neutral IGM beyond the redshift of reionization, the collapsed fraction should be computed for halos of sufficient mass to initiate star formation. The critical virial temperature is set by the temperature ( $T_N \sim 10^4$  K) above which efficient atomic hydrogen cooling promotes star formation. Following the reionization of a region, the Jeans mass in the heated IGM limits accretion to halos above  $T_1 \sim 10^5$  K (Efstathiou 1992; Thoul & Weinberg 1996; Dijkstra et al. 2004). We may therefore write the time derivative of the collapsed fraction

$$\begin{aligned} \frac{dF}{dt_{\text{year}}}(z) &= \left[ Q_m(z) \frac{dF(z, T_1)}{dz} + [1 - Q_m(z)] \frac{dF(z, T_N)}{dz} \right] \\ &\quad \times \frac{dz}{dt_{\text{year}}}, \end{aligned} \quad (6)$$

where  $Q_m$  is the ionized mass fraction in the universe.

To describe the ionizing flux from stars we require one additional parameter. Only a fraction of ionizing photons produced by stars may enter the IGM. Therefore an additional factor of  $f_{\text{esc}}$  (the escape fraction) must be included when computing the emissivity of galaxies. Ciardi & Ferrara (2005) include a review of existing constraints on  $f_{\text{esc}}$  which suggests that its value is  $\lesssim 15\%$ . More recent simulations (Gnedin, Kravtsov, & Chen 2007) show the average escape fraction from galaxies to be only a few percent over a wide redshift range. The product of the star formation efficiency and the escape fraction may be combined into a single free parameter ( $f_{\star, \text{esc}} = f_\star \times f_{\text{esc}}$ ) to describe the contribution of stars in our model. The ionizing photon emissivity

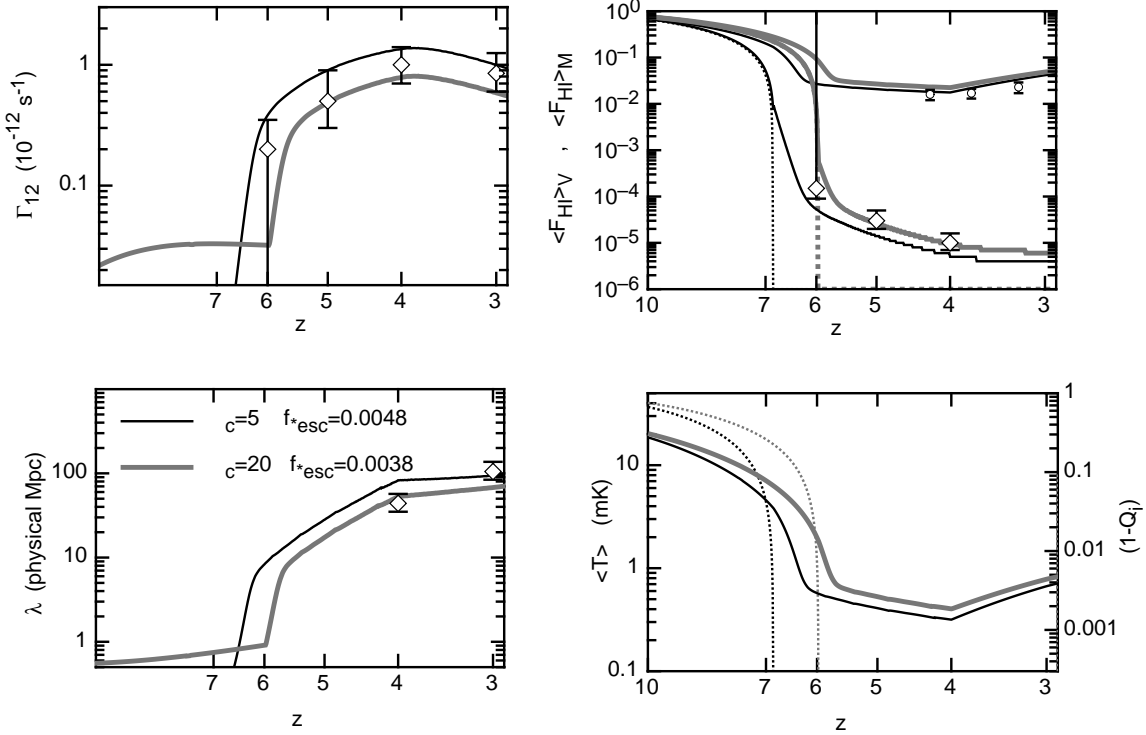


**Figure 1.** Models for the reionization of the IGM and the subsequent post-overlap evolution of the ionizing radiation field. In each panel two cases are shown, corresponding to different values for the critical overdensity prior to the overlap epoch ( $\Delta_c = 5$ , thin dark lines; and  $\Delta_c = 20$ , thick grey lines). We show the cases for the mean IGM with  $\delta = 0$ . *Upper Left Panel:* The ionization rate as a function of redshift. The observational points are from Bolton et al. (2007b). *Upper Right Panel:* The volume (lower curves) and mass (upper curves) averaged fractions of neutral gas in the universe. Also shown (dotted lines) is the fraction of the IGM yet to overlap ( $1 - Q_i$ ). The observational points for the volume averaged neutral fraction are from Bolton et al. (2007b), while the observed mass-fractions are from the damped Ly $\alpha$  measurements of Prochaska et al. (2005). *Lower Left Panel:* The mean-free-path for ionizing photons computed using the formalism in § 2. The data points are based on Storrie-Lombardi et al. (1994). *Lower Right Panel:* The evolution of the mean 21cm brightness temperature (in mK) with redshift (solid lines). For comparison, the fraction of IGM yet to overlap ( $1 - Q_i$ ) is overplotted.

may then be written as

$$\frac{dn_\gamma}{dt} = f_{*,\text{esc}} N_\gamma \frac{dF}{dt}(z) \rho_b, \quad (7)$$

where  $\rho_b$  is the co-moving mass-density of baryons.

### 3 RESULTS

Figure 1 shows example models for the reionization of the IGM and the subsequent post-overlap evolution of the ionizing radiation field. Two cases are shown, corresponding to two different values for the critical overdensity prior to the overlap epoch ( $\Delta_c = 5$  and  $\Delta_c = 20$ ), with values of  $f_{*,\text{esc}} = 0.0048$  and  $f_{*,\text{esc}} = 0.0038$  respectively. These cases do not represent the best fit to the data, but rather bracket the range of the overlap epoch redshifts ( $6 \lesssim z \lesssim 7$ ) for which our model is consistent with observations at  $z \lesssim 6$  (without invoking an additional population of more massive stars at high redshift; e.g. Wyithe & Loeb 2003). The examples have different values of  $\Delta_c$ , and thus illustrate the mild dependence of our results on this unknown parameter. We note that the values of  $f_{*,\text{esc}}$  required for our model to reproduce existing observations are in excellent agreement with external considerations. In particular our value of  $f_{*,\text{esc}} \sim \text{a few } \times 10^{-3}$  corresponds to product of recent

estimates for the escape fraction (a few  $\times 10^{-2}$ ; Gnedin, Kravtsov, & Chen 2007), with estimates of the average star-formation rate ( $\sim 10^{-1}$  from the ratio between the mass density in stars and baryons; Fukugita, Hogan & Peebles 1998).

In the top left panel of Figure 1 we show the evolution of the ionization rate. The observational points are from the simulations of Bolton et al. (2007b; based on the observations of Fan et al. 2006). In the top-right panel we plot the corresponding volume (lower curves) and mass (upper curves) averaged fractions of neutral gas in the universe. Also shown (dotted lines) is the fraction of the IGM yet to overlap ( $1 - Q_i$ ). The redshift where these curves drop to zero is normally quoted as the redshift of reionization, and these curves correspond approximately to the standard semi-analytic calculation (e.g. Haiman & Loeb 1997). However our formalism allows for the calculation of both mass and volume averaged neutral fractions to lower redshifts. The observational points for the volume averaged neutral fraction are from Bolton et al. (2007b), while the observed mass-fractions are from the damped Ly $\alpha$  measurements of Prochaska et al. (2005), and therefore represent lower limits on the total HI content of the IGM. Both curves show excellent agreement with these quantities, despite their differing by 3 orders of magnitude. In the lower left panel we plot the evolution of the ionizing photon mean-free-path. The data

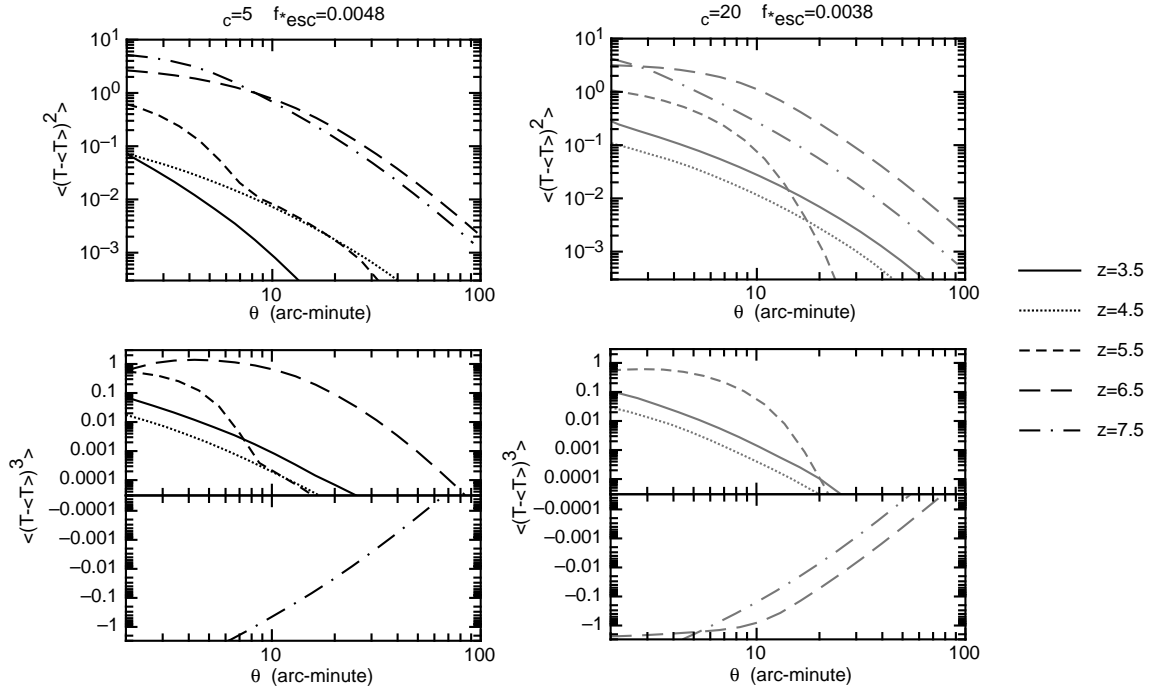


**Figure 2.** Examples of auto-correlation and skewness functions. *Upper Panels:* The auto-correlation is plotted as a function of  $\theta$  at 5 different redshifts spanning the overlap epoch (for this model). *Lower Panels:* The corresponding examples of skewness functions. Two cases are shown, corresponding to different values for the critical overdensity prior to the overlap epoch ( $\Delta_c = 5$ , left panels; and  $\Delta_c = 20$ , right panels).

points are based on Storrie-Lombardi et al. (1994). Again the model is in good agreement with the available observations. We note that the observed mean-free-path is found from the number density of Ly-limit systems and is independent of the Ly $\alpha$  forest absorption derived quantities of ionization rate and volume averaged neutral fraction, as well as being independent of the HI mass-density measurements. Our simple model therefore simultaneously reproduces the evolution of three independent measured quantities.

At a specified redshift, our model yields the mass-averaged fraction of ionised regions within the IGM on various scales  $R$  as a function of overdensity. We may then calculate the corresponding 21cm brightness temperature contrast

$$T(\delta, R) = 22\text{mK} \left( \frac{1+z}{7.5} \right)^{1/2} (1 - Q_i F_M(\Delta_i, \delta, R)) \left( 1 + \frac{4}{3}\delta \right), \quad (8)$$

where the pre-factor of 4/3 on the overdensity refers to the spherically averaged enhancement of the brightness temperature due to peculiar velocities in overdense regions (Bharadwaj & Ali 2005; Barkana & Loeb 2005). In the lower right panel of Figure 1 we show the evolution of the mean brightness temperature contrast of 21cm emission with redshift. For comparison, we also show the fraction of IGM yet to overlap. Significant mean redshifted 21cm emission will extend for at least a redshift unit beyond overlap (during which time it has dropped by a factor of  $\sim 5$ ). This implies that a global step signature will be very gradual, making its detection by instruments with a limited band-pass challenging.

### 3.1 Fluctuations in 21cm emission

Given the distribution of  $\delta$  from the primordial power-spectrum of density fluctuations, we may find the probability distribution  $dP/dT$  of brightness temperature  $T$  in redshifted 21cm intensity maps, and hence the second and third moments of the distribution as functions of angular scale and redshift (Wyithe & Morales 2007). The structure of our semi-analytic model for reionisation makes it natural to discuss the moments of the real space intensity fluctuations smoothed within top-hat window functions of angular radius  $\theta$ .

The second moment of these distributions corresponds to the auto-correlation function of brightness temperature smoothed on an angular radius  $\theta$ :

$$\langle (T - \langle T \rangle)^2 \rangle = \left[ \frac{1}{\sqrt{2\pi}\sigma(R)} \int d\delta (T(\delta, R) - \langle T \rangle)^2 e^{-\frac{\delta^2}{2\sigma(R)^2}} \right], \quad (9)$$

where

$$\langle T \rangle = \frac{1}{\sqrt{2\pi}\sigma(R)} \int d\delta T(\delta, R) e^{-\frac{\delta^2}{2\sigma(R)^2}}, \quad (10)$$

and  $\sigma(R)$  is the variance of the density field (at redshift  $z$ ) smoothed on a scale  $R$ .

A measure of the departure of the statistics from those of a Gaussian random field is provided by the third moment of the distribution  $dP/dT$ . We refer to the third moment as the skewness function of brightness temperature smoothed

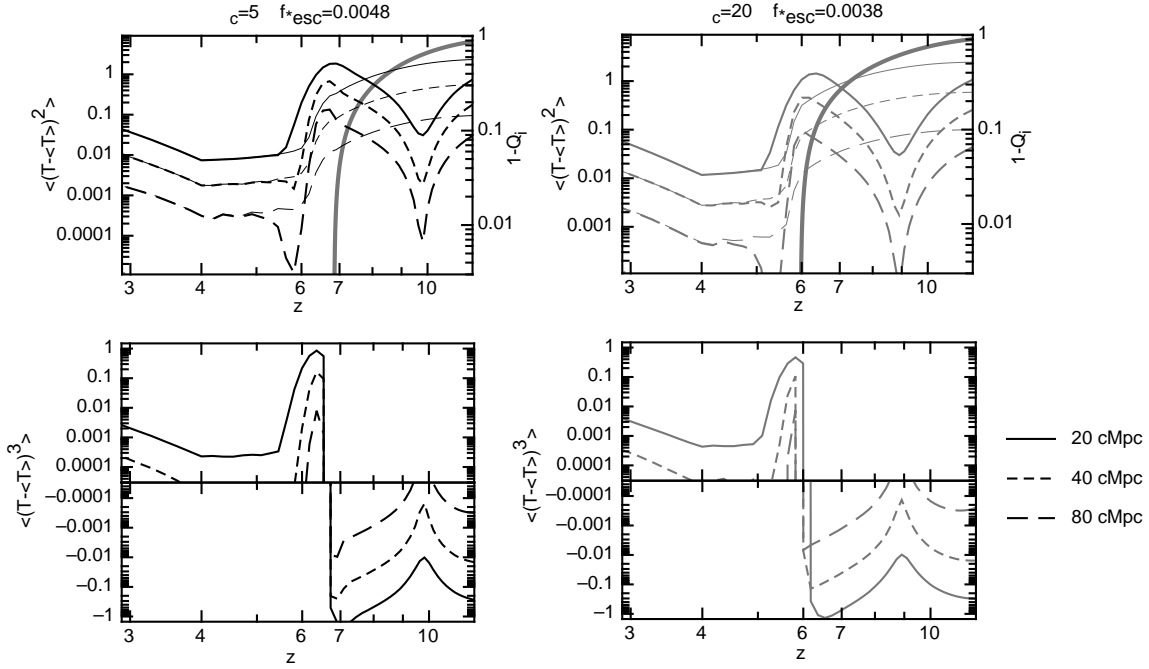


**Figure 3.** Examples of auto-correlation and skewness functions. Two cases are shown, corresponding to different values for the critical overdensity prior to the overlap epoch ( $\Delta_c = 5$ , left panels; and  $\Delta_c = 20$ , right panels). *Upper Panels:* The auto-correlation is plotted as a function of redshift for 3 different co-moving scales of relevance for observations using upcoming low-frequency radio telescopes. The heavy lines show our model. For comparison the thin lines show the fluctuations in the absence of galaxy bias. Also shown for comparison is the fraction of IGM yet to overlap (thick grey line dropping to zero at  $z = 6 - 7$ ). *Lower Panels:* The corresponding examples of skewness functions.

with top-hat windows of angular radius  $\theta$ :

$$\langle (T - \langle T \rangle)^3 \rangle = \left[ \frac{1}{\sqrt{2\pi}\sigma(R)} \int d\delta (T(\delta, R) - \langle T \rangle)^3 e^{-\frac{\delta^2}{2\sigma(R)^2}} \right]. \quad (11)$$

Examples of auto-correlation and skewness functions are plotted in Figure 2. The upper panels show the auto-correlation plotted as a function of  $\theta$  at 5 different redshifts spanning the overlap epoch (for this model). The lower panels show the corresponding examples of skewness functions. Further examples of auto-correlation and skewness functions are plotted in Figure 3, but this time as a function of redshift for 3 different co-moving scales of relevance for upcoming low-frequency radio telescopes. The thick dark lines show the evolution for our full model. We also show (thin dark lines) the fluctuations that would be present in the absence of galaxy bias. Comparison of these curves demonstrates that galaxy bias is important in setting fluctuation levels prior to the overlap epoch, but becomes progressively less important after the overlap epoch is completed. This is because the mean-free-path becomes large following the completion of overlap, and as a result the ionizing photons that form the background at a particular location in the IGM are then drawn from a volume that is much larger than the regions among which the fluctuations are measured. Galaxy bias remains important until lower redshifts on larger scales  $R$  because the mean-free-path exceeds  $R$  only at later times. Also shown for comparison (heavy grey lines) is the fraction of IGM yet to overlap ( $1 - Q_i$ ).

Figures 2-3 suggest that a characteristic feature of the overlap epoch will be the inversion of the 21cm intensity dis-

tribution from negative to positive skewness. As mentioned above, the ionization state of an overdense region is set by the competing effects of galaxy bias, and higher gas density (and recombination rate). With respect to 21cm fluctuations, this inversion therefore corresponds to the shift in dominance from the biased radiation field prior to the overlap epoch, to dominance of gas density and recombinations on small scales after the overlap epoch (when the long ionizing mean-free path washes out the effect of galaxy bias).

To investigate the sensitivity of forthcoming low-frequency telescopes to the fluctuations in 21cm emission after reionization, we have estimated the signal-to-noise for the Mileura-Widefield Array (MWA<sup>1</sup>) using the formalism outlined in Wyithe & Morales (2007). The MWA, which is currently under construction will comprise a phased array of 500 tiles (each tile will contain 16 cross-dipoles) distributed over an area with diameter 1.5km. In Figure 4 we show examples of signal-to-noise for auto-correlation and skewness functions measured with the MWA assuming 1000 hours integration (the examples correspond to the models in Figure 3). In the upper panels we plot the signal-to-noise for the auto-correlation as a function of redshift for 3 different co-moving scales of relevance for the MWA. Also shown for comparison as before is the fraction of IGM yet to overlap ( $1 - Q_i$ ). In the lower panels we show the corresponding signal-to-noise for the skewness function. The model suggests that the auto-correlation will reach a minimum around a redshift unit following the completion of the overlap epoch,

<sup>1</sup> see <http://www.haystack.mit.edu/ast/arrays/mwa/index.html>

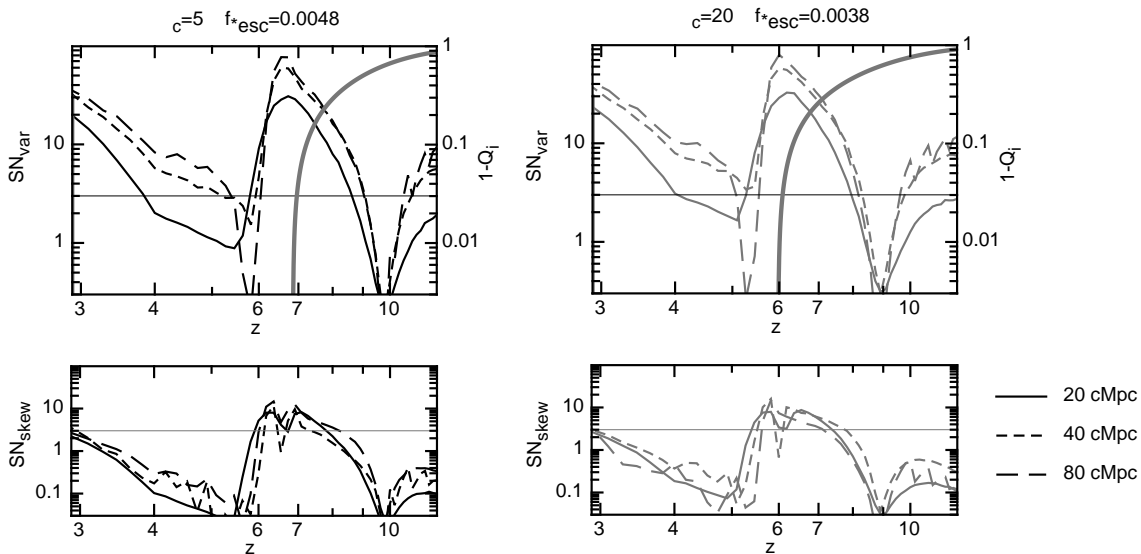


**Figure 4.** Examples of signal-to-noise for auto-correlation and skewness functions measured with the MWA assuming 1000 hours integration. Two cases are shown, corresponding to different values for the critical overdensity prior to the overlap epoch ( $\Delta_c = 5$ , left panels; and  $\Delta_c = 20$ , right panels). *Upper Panels:* The signal-to-noise for the auto-correlation function is plotted as a function of redshift for 3 different co-moving scales of relevance for observations using upcoming low-frequency radio telescopes. Shown for comparison is the fraction of IGM yet to overlap according to the definition in § 2 (thick grey lines). *Lower Panels:* The corresponding examples of signal-to-noise for skewness functions. Horizontal lines have been drawn at a signal-to-noise of 3 to guide the eye.

but that even here it will remain detectable at a signal-to-noise of several. Moreover the signal-to-noise at  $z \sim 3 - 4$  should be comparable with that near the peak of the reionization era due to the decreased level of sky-noise at lower redshifts. The MWA is designed to be sensitive to frequencies as high as 300MHz, or redshifts as low as  $z \sim 3.5$ . Thus redshifted 21cm observations could be used to track the entire overlap era into the post reionization IGM.

#### 4 THE POWER-SPECTRUM OF 21CM FLUCTUATIONS AFTER REIONIZATION

Our analysis thus far has concentrated on the auto-correlation function of 21cm fluctuations. A more powerful statistical probe will be provided by the power-spectrum which is naturally accessible to interferometric observations such as those to be carried out by the MWA. During the reionization epoch, the relation between the power-spectrum of 21cm fluctuations and the underlying matter power-spectrum is complex, and in the late stages is dominated by the formation of large ionized bubbles (Furlanetto et al. 2004; McQuinn et al. 2006). After reionization (i.e.  $z \lesssim 5.5$ ) there are no longer separate ionized bubbles as most of the IGM is ionized. Our modeling suggests that the skewness of the 21cm intensity fluctuation distribution will be small during the post overlap epoch. As a result the 21cm emission will follow the density field up to a constant of proportionality whose value reflects the neutral fraction and a bias like factor due to the varying rate of recombination with overdensity. Thus, after the overlap of HII regions we may write the following expression for the power-spectrum of 21cm fluctuations

$$P_{21}(k) = b_{21}^2 P(k) D(z)^2, \quad (12)$$

where  $P(k)$  is the primordial power-spectrum of the density field, extrapolated linearly to  $z = 0$ . The bias  $b_{21}$ , which has dimensions of temperature squared may be determined directly from our calculation of the auto-correlation function, i.e.

$$b_{21}(R)^2 = \frac{\langle (T - \langle T \rangle)^2 \rangle}{\sigma(R)^2}. \quad (13)$$

The bias  $b_{21}$  is a function of  $R$ , but at  $z \lesssim 5$  is nearly independent of scale over the range of interest. We show examples of the resulting power-spectrum (thick solid lines) in Figure 5 at  $z = 3.5$  (left panels) and  $z = 5$  (right panels). The model power-spectrum shown was computed assuming  $\Delta_c = 20$ , for which we find  $b_{21} \sim 1.2\text{mK}$  at both  $z = 3.5$  and  $z = 5$ .

Calculations of the sensitivity to the 21cm power-spectrum for an interferometer have been presented by a number of authors. We follow the procedure outlined by McQuinn et al. (2006), drawing on results from Bowman, Morales & Hewitt (2006) for the dependence of the array antenna density on radius  $\rho(r)$ . The uncertainty in a measurement of the power-spectrum has two separate components, due to the thermal noise of the instrument ( $\Delta P_{21,N}$ ), and due to sample variance within the finite volume of the survey ( $\Delta P_{21,sv}$ ). The contamination of foregrounds provides an additional source of uncertainty in the estimate of the power-spectrum. McQuinn et al. (2006) have shown that it should be possible to remove the power due to foregrounds to a level below the cosmological signal, provided that the region of band-pass from which the power-spectrum is estimated is substantially smaller than the total band-pass available. Following the approximation suggested in McQuinn et al. (2006), we combine the above components to

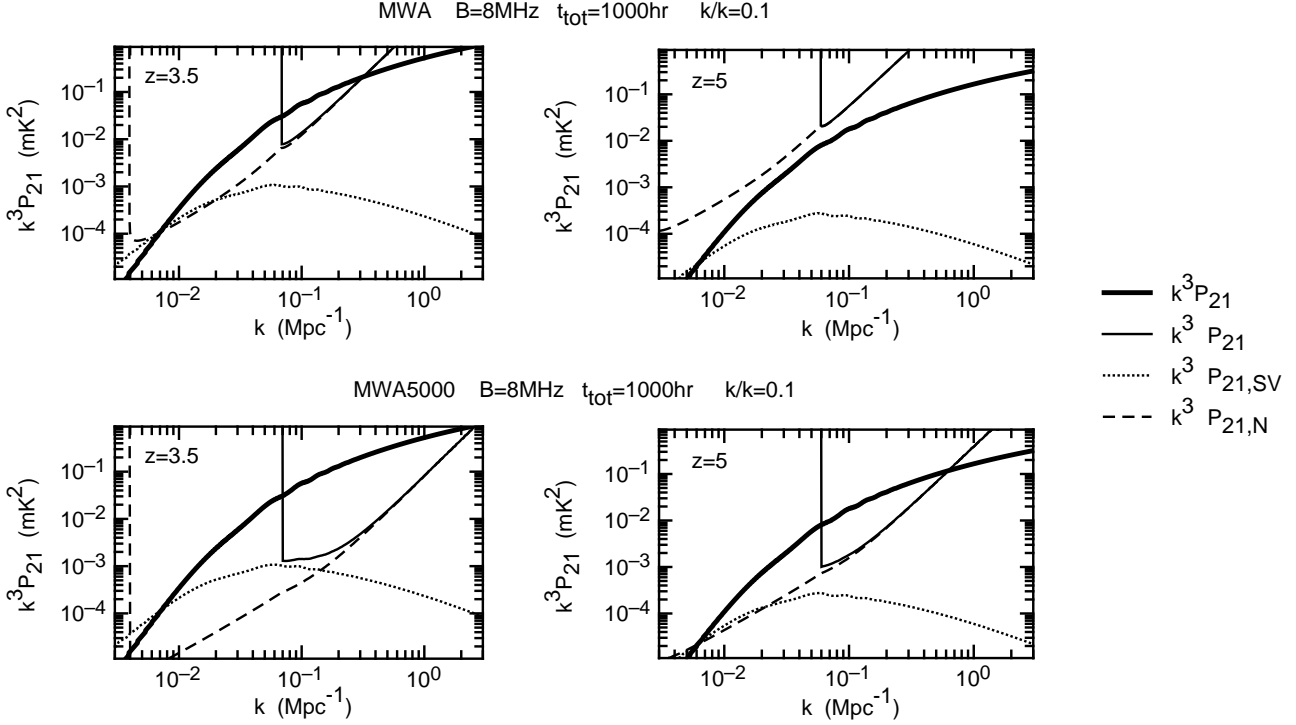


**Figure 5.** The power-spectrum of 21cm fluctuations after reionization (thick solid lines) at  $z = 3.5$  (left panels) and  $z = 5$  (right panels). The model power-spectrum shown was computed assuming  $\Delta_c = 20$ . Also shown for comparison are estimates of the noise for MWA (upper panels) and its future extension MWA5000 (lower panels). In each case we plot the sample-variance (dotted lines) and thermal noise (dashed lines) components of the uncertainty within  $k$ -space bins of size  $\Delta k = k/10$ . The combined uncertainty including the minimum  $k$  cutoff due to foreground subtraction, is also shown as the thin solid lines.

yield the uncertainty on the estimate of the power-spectrum

$$\begin{aligned} \Delta P_{21} &= \Delta P_{21,SV} + \Delta P_{21,N} \quad \text{if } k > k_{\min} \\ &= \infty \quad \text{otherwise} \end{aligned} \quad (14)$$

where  $k_{\min} = 2\pi/y$  and  $y$  is the co-moving line-of-sight distance corresponding to the band-pass within which the power-spectrum is measured.

Estimates of the sample-variance (dotted lines) and thermal noise (dashed lines) components of the uncertainty for detection by the MWA are plotted in the upper panels of Figure 5. We model the antennae distribution as having  $\rho(r) \propto r^{-2}$  with a maximum radius of 750m and a finite density core of radius 20m, and we assume a 1000hr integration, a bandpass of  $B = 8\text{MHz}$ , and  $k$ -space bins of width<sup>2</sup>  $\Delta k = k/10$ . The combined uncertainty including the minimum  $k$  cutoff due to foreground subtraction is shown as the thin solid line. The results confirm our expectations based on results in the previous section. The power-spectrum of 21cm fluctuation should be detectable at high significance at  $z \sim 3.5$ , well after the completion of reionization. Indeed the signal-to-noise for detection of the power-spectrum at  $z \sim 3.5$  is not dissimilar to expectations for the signal-to-noise during the reionization era itself (e.g. McQuinn et al. 2006). On the other hand, due to the increasing sky dom-

inated system-noise at higher redshift, a detection will be more challenging at redshifts just after overlap.

At values of  $k \sim \text{a few} \times 10^{-1} \text{ Mpc}^{-1}$ , the measurement of the power-spectrum using the MWA will be limited by the thermal sensitivity of the array, and so the signal-to-noise achievable in this regime will be greatly enhanced by a subsequent generation of instruments with larger collecting area. As an example we consider a hypothetical followup instrument to the MWA which would comprise 10 times the total collecting area. We refer to this followup telescope as the MWA5000. The design philosophy for the MWA5000 would be similar to the MWA, and we therefore assume antennae distributed as  $\rho(r) \propto r^{-2}$  with a diameter of 2km and a flat density core of radius 80m (see McQuinn et al. 2006). In the lower panels of Figure 5 we present estimates for measurement of the 21cm power-spectrum using MWA5000. The sample-variance (dotted lines) and thermal noise (dashed lines) components of the uncertainty are plotted as before assuming a 1000hr integration, a bandpass of  $B = 8\text{MHz}$ , and  $k$ -space bins of width  $\Delta k = k/10$ . The combined uncertainty including the minimum  $k$  cutoff due to foreground subtraction is shown as the thin solid line. This figure, in combination with previous calculations of sensitivity to the 21cm power-spectrum during reionization (e.g. McQuinn et al. 2006) demonstrates that the MWA5000 could measure the 21cm power-spectrum in detail across the entire frequency range accessible to an MWA antennae, corresponding to a redshift range of  $3.5 \lesssim z \lesssim 15$ .

The reionization epoch has formed the dominant driver for studies of the statistical properties of redshifted 21cm

<sup>2</sup> The signal-to-noise is increased in proportion to  $\sqrt{\Delta k}$ , and so will be substantially better per bin in measurements of the power-spectrum at lower resolution in  $k$ .



emission to date, while we have argued in this paper that the study of the IGM using 21cm emission could also be extended to lower post-reionization redshifts. However the measurement of a 21cm power spectrum will also provide significant cosmological information (McQuinn et al. 2006). For example the angular scale of the baryonic acoustic peak in the matter power spectrum, measured through redshifted 21cm observations could be used to constrain the evolution of the dark energy with cosmic time (Blake & Glazebrook 2003; Seo & Eisenstein 2007; Angulo et al. 2007) in the redshift range of  $3.5 \lesssim z \lesssim 6$ , as well as during the reionization era. No other probes are currently effective during these epochs (Corasaniti, Huterer, & Melchiorri 2007). A detailed analysis of the prospects for such a study with future low-frequency arrays will be presented elsewhere.

## 5 DISCUSSION

While the recent discovery of distant quasars has allowed detailed absorption studies of the state of the IGM at  $z \sim 6$  (Fan et al. 2006; White et al. 2003), the interpretation of the data is not yet robust. The prime reason for the ambiguity in interpreting high redshift quasar absorption spectra is that Ly $\alpha$  absorption can only be used to probe volume averaged neutral fractions that are smaller than  $10^{-3}$ , owing to the large cross-section of the Ly $\alpha$  resonance. A better probe of the process of reionization is provided by redshifted 21cm observations. The conventional wisdom is that the 21cm signal disappears after the *overlap* epoch, because there is little neutral hydrogen left through most of the intergalactic space. But observations of damped Ly $\alpha$  systems out to redshift  $z \sim 4$  show the density parameter of HI to be  $\Omega_{\text{HI}} \sim 10^{-3}$ , indicating that the mass averaged neutral hydrogen fraction remains at the level of a few percent throughout cosmic history.

Existing constraints from Ly $\alpha$  studies are based on line-of-sight averaged optical depths and are therefore sensitive to the volume filling fraction of neutral hydrogen. These observations are limited in their ability to probe the IGM once the overlap era is approached due to the high optical depth to Ly $\alpha$  absorption. On the other hand, redshifted 21cm observations directly probe the pockets where most of the hydrogen resides after reionization. In this paper we have considered the detection of fluctuations in 21cm emission from neutral hydrogen after the completion of reionization using low-frequency telescopes that are currently under construction (specifically the Mileura Widefield Array, MWA). Based on a physically motivated model for the reionization era we have shown that the residual neutral gas, which is contained in high density pockets following the end of the overlap epoch, produces a substantial signal of 21cm fluctuations. These fluctuations directly probe the post-reionization IGM and have a power-spectrum that will be detectable by the MWA at a signal-to-noise ratio that is comparable to observations during the reionization epoch. We stress that in the case of observations at  $z \lesssim 5$  the prediction of the power-spectrum amplitude is quite robust, being primarily dependent on the underlying mass power-spectrum and the mass-averaged neutral fraction of hydrogen which, unlike predictions for the reionization epoch, represent well-measured quantities.

Models of reionization predict that non-Gaussianity in the distribution of 21cm intensities would be the signature of star-formation driven reionization of the IGM. Our calculations predict that after the overlap of HII regions in the IGM, there will be a transition between an epoch of negative skewness when the statistics of the intensity distribution are driven by galaxy-bias (prior to overlap), and an epoch of positive skewness when they are driven by the density distribution and recombination rate (post-overlap). Observation of this rapid transition in the statistics of the 21cm signal will therefore provide added confidence that the end of the reionization era has been detected.

Observations of the post-reionization 21cm power-spectrum will be significantly enhanced by 2nd generation low-frequency telescopes with increased collecting area. In addition to the utility of 21cm fluctuations for studies of the evolution in the ionization state of the IGM during the post reionization epoch, measurement of the 21cm power-spectrum may therefore yield precise measurements of the angular scale of the acoustic peak in the matter power-spectrum. Thus in the future it may become possible to use redshifted 21cm studies to constrain the dark energy in the unexplored redshift range of  $3.5 \lesssim z \lesssim 15$ , where it is not accessible through other techniques.

**Acknowledgments** The research was supported by the Australian Research Council (JSBW) and Harvard University grants (AL). AL thanks the astrophysicists at Caltech for their kind hospitality as the Kingsley visitor during the completion of this work.

## REFERENCES

- Angulo, R., Baugh, C. M., Frenk, C. S., & Lacey, C. G. 2007, ArXiv Astrophysics e-prints, arXiv:astro-ph/0702543
- Barkana, R., Loeb, A. 2001, Phys. Rep., 349, 125
- Barkana, R., & Loeb, A. 2005 ApJL, 624, L65
- Becker, G. D., Rauch, M., & Sargent, W. L. W. 2007, ApJ, 662, 72
- Bharadwaj, S., & Ali, S. S. 2005, MNRAS, 356, 1519
- Blake, C., & Glazebrook, K. 2003, ApJ, 594, 665
- Bolton, J. S., & Haehnelt, M. G. 2007a, MNRAS, 374, 493
- Bolton, J. S., & Haehnelt, M. G. 2007b, submitted to MNRAS
- Bond, J. R., Cole, S., Efstathiou, G., & Kaiser, N. 1991, ApJ, 379, 440
- Bowman, J. D., Morales, M. F., & Hewitt, J. N. 2006, ApJ, 638, 20
- Ciardi, B., Ferrara, A. 2005, Space Sc. Rev., 116, 625
- Corasaniti, P.-S., Huterer, D., & Melchiorri, A. 2007, Phys. Rev. D, 75, 062001
- Curran, S. J., Tzanavaris, P., Murphy, M. T., Webb, J. K., & Pihlstrom, Y. M. 2007, ArXiv e-prints, 706, arXiv:0706.2692
- Dijkstra, M., Haiman, Z., Rees, M. J., & Weinberg, D. H. 2004, ApJ, 601, 666
- Efstathiou, G. 1992, Mon. Not. R. Astron. Soc., 256, 43
- Fan, X., et al. 2006, AJ, 132, 117
- Fukugita, M., Hogan, C. J., & Peebles, P. J. E. 1998, ApJ, 503, 518
- Furlanetto, S. R., & Loeb, A. 2002, ApJ, 579, 1

- Furlanetto, S. R., Zaldarriaga, M., & Hernquist, L. 2004, *ApJ*, 613, 16
- Gnedin, N. Y., & Fan, X. 2006, *ApJ*, 648, 1
- Gnedin, N. Y., Kravtsov, A. V., & Chen, H.-W. 2007, *ArXiv e-prints*, 707, arXiv:0707.0879
- Haiman, Z., & Loeb, A. 1997, *ApJ*, 483, 21
- Kanekar, N., & Chengalur, J. N. 2003, *Astron. Astrophys.*, 399, 857
- Leitherer, C., et al. 1999, *ApJS*, 123, 3
- Lidz, A., McQuinn, M., Zaldarriaga, M., Hernquist, L., & Dutta, S. 2007, *ArXiv Astrophysics e-prints*, arXiv:astro-ph/0703667
- McQuinn, M., Zahn, O., Zaldarriaga, M., Hernquist, L., & Furlanetto, S. R. 2006, *ApJ*, 653, 815
- Mesinger, A., Haiman, Z., & Cen, R. 2004, *ApJ*, 613, 23
- Miralda-Escudé, J., Haehnelt, M., & Rees, M. J. 2000, *ApJ*, 530, 1
- Press, W., Schechter, P. 1974, *ApJ.*, 187, 425
- Prochaska, J. X., Herbert-Fort, S., & Wolfe, A. M. 2005, *ApJ*, 635, 123
- Seo, H.-J., & Eisenstein, D. J. 2007, *ApJ*, 665, 14
- Spergel, D. N., et al. 2007, *ApJS*, 170, 377
- Srbínovsky, J. A., & Wyithe, J. S. B. 2007, *MNRAS*, 374, 627
- Storrie-Lombardi, L. J., McMahon, R. G., Irwin, M. J., & Hazard, C. 1994, *ApJL*, 427, L13
- Thoul, A. A., & Weinberg, D. H. 1996, *Astrophys. J.*, 465, 608
- White, R., Becker, R., Fan, X., Strauss, M. 2003, *Astron J.*, 126, 1
- Wyithe, J. S. B, Bolton, J. S., Haehnelt, M. 2007, *MNRAS*, submitted
- Wyithe, J. S. B, Loeb, A. 2003, *ApJ*, 586, 693
- Wyithe, J.S.B, Loeb, A. 2004, *Nature*, 427, 815
- Wyithe, J.S.B, Loeb, A., Carilli, C. 2005, *ApJ*, 628, 575
- Wyithe, S., & Morales, M. 2007, *ArXiv Astrophysics e-prints*, arXiv:astro-ph/0703070